Inorganic Chemistry

pubs.acs.org/IC
Article

Water-Mediated Chiral Resolution of Ag−NHC(Nucleobase) Complexes

Alvaro Polo, Ricardo Rodríguez, Ramón Macías, Daniel Cobo Paz, and Pablo J. Sanz Miguel*

Cite This: *Inorg. Chem.* 2025, 64, 5487−5494
Read Online

ACCESS | Metrics & More | Article Recommendations | Supporting Information

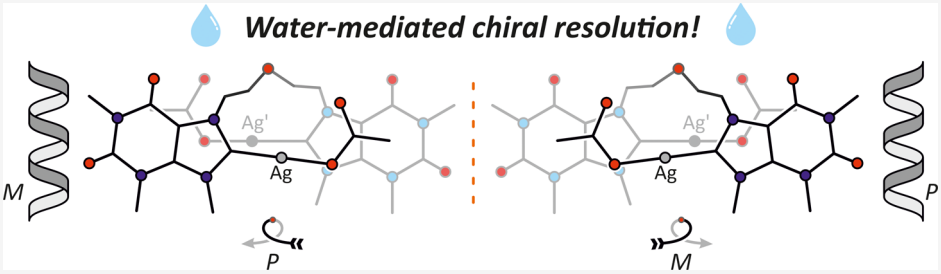

ABSTRACT: This study reveals a novel role of water as a chiral inducer, demonstrating its ability to drive the asymmetric resolution of prochiral silver-nucleobase complexes. During crystallization, helical water columns spontaneously form, selectively recognizing one enantiomer of the silver complex. This enantiospecific interaction drives the separation of the *P* and *M* enantiomers, leading to the formation of enantiopure crystals, whose chirality was confirmed through X-ray crystallography.

INTRODUCTION

Water is the most abundant inorganic compound in nature, found both in the Earth's crust and within living organisms. Hydrogen bonding,[1] which is responsible for the primary structural cohesion between water dipoles, also drives the formation of water clusters.[2−5] Their arrangement has been elucidated in the gaseous, liquid, and solid phases, revealing intricate geometric configurations, including discrete and polymeric constructs such as linear chains, tapes, nanotubes, layers, or three-dimensional structures.[6,7]

Water clusters typically build in the interstices of crystalline networks, filling the voids left by crystallizing molecules, thereby providing stability and, in many cases, modifying or even governing the molecular arrangement. More importantly, water clusters play a key role in many biological processes, such as protein folding, enzyme activity, or DNA stability, actively influencing their structure and properties.[8−16] In this regard, it is expected that a water cluster assembled around a DNA fragment will adopt its inherent chirality.[17,18] This concept can be extended to the environs of other chiral natural and artificial systems, in which chirality is transferred from an organic or metal−ligand template to a well-defined water network.[19−25] Conversely, water clusters can also induce the assembly of supramolecular nanostructures and tune their optical properties.[26]

In recent years, the use of purine nucleobases as *N*-heterocyclic carbene (NHC) ligands has been increasingly explored.[27−29] Most reports have focused on the antiproliferative activity of caffeine- and theophylline-based metal complexes.[30−35] Additionally, the use of these bioinspired ligands has been expanded to catalytically[36−38] and optically[39] active systems as a greener and more sustainable alternative[40] to traditional NHCs.

Our interest in metal-nucleobase complexes, led us to design and investigate flexible nucleobase- and *N*-donor based ligands.[41−45] In this study, a bidentate ligand (**2**), in which two theophylline synthons are linked by a $-CH_2-CH_2-O-CH_2-CH_2-$ ether group, assembles into a dinuclear silver complex (**3**) with intrinsic chirality. During the crystallization process of **3**, spontaneous formation of helical water columns occurs, in which the water selectively recognizes a homoenantiomer of complex **3** over the other. This recognition promotes the growth of enantiopure crystals and enables the chiral resolution of **3**.

RESULTS AND DISCUSSION

Ligand bis[2-(7-theophyllinyl)ethyl]ether (**1**), was conveniently prepared in *N*,*N*-dimethylformamide (DMF) by reacting theophylline with bis(2-chloroethyl)ether (Scheme 1). Addition of water to the DMF solution prompted the precipitation of **1**, which was isolated by filtration in air. A further reaction of **1** with methyl triflate (MeOTf) allowed for the methylation of

Received: December 17, 2024
Revised: January 22, 2025
Accepted: February 3, 2025
Published: February 10, 2025

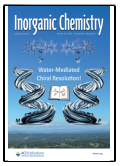

https://doi.org/10.1021/acs.inorgchem.4c05384
Inorg. Chem. 2025, 64, 5487−5494

Scheme 1. Formation of Compounds 1, 2[OTf]$_2$, 2[Br]$_2$, and 3[a]

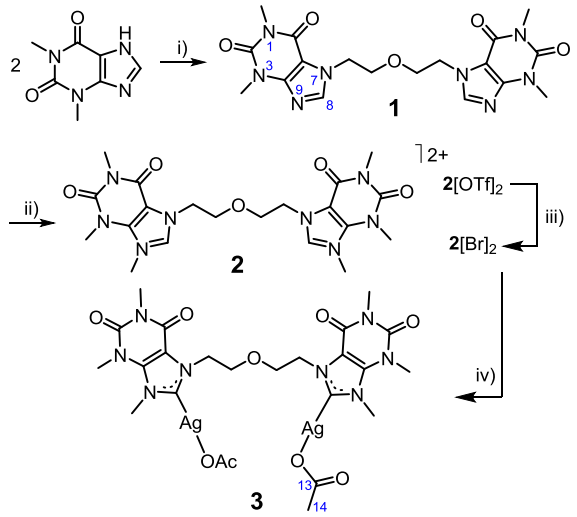

[a](i) 0.5 eq bis(chloroethyl)ether, NaOH, DMF, 80 °C; (ii) 2 eq MeOTf, CH_2Cl_2, RT; (iii) [TBA]Br, THF, RT; (iv) 4 eq [Ag(OAc)], CH_2Cl_2, RT.

the N9 sites of the two purine bases, with the subsequent formation of the triflate salt, 2[OTf]$_2$ (Scheme 1). In order to introduce a more suitable anion (Br^-) into the medium for the ensuing treatment with silver, NBu_4Br was added to a solution of 2[OTf]$_2$, facilitating the isolation of 2[Br]$_2$. Finally, metalation of both C8 positions of theophylline fragments by Ag^+ units was achieved upon treatment of 2[Br]$_2$ with silver acetate, [Ag(OAc)], yielding [$Ag_2(OAc)_2$(**2**$_{-2H}$)] (**3**).

NMR Analysis. The ^{1}H NMR spectrum of **1** ($CDCl_3$, Supporting Information) is consistent with a symmetrical (theophylline-*N*7)−CH_2−CH_2−O−CH_2−CH_2−(theophylline-*N*7) array. *N*1-CH_3 and *N*3-CH_3 methyl groups are observed as singlets at 3.34 and 3.55 ppm, whereas the *N*7-CH_2 and *O*-CH_2 signals appear at 4.37 and 3.71 ppm, respectively. Besides, the H8 proton resonates as a singlet at 7.40 ppm. Further NMR characterization is provided in the Supporting Information: ^{1}H−^{1}H COSY, ^{13}C{^{1}H}-APT, ^{1}H−^{13}C HSQC, and ^{1}H−^{13}C HMBC spectra.

In 2[OTf]$_2$, the presence of methyl groups at the N9 sites of theophylline and the resulting positive charge, delocalized in the heterocyclic rings,[46] provoke the expected shift of the peaks in the ^{1}H NMR spectrum. This is more pronounced in those attached to the imidazolium ring, *N*7-CH_2 (4.67 ppm) and *N*9-CH_3 (4.14 ppm). In addition, the shift of the H8 signal (8.79 ppm) confirms methylation at the neighboring N9 position. Moreover, 2[Br]$_2$ displays a ^{1}H NMR pattern similar to that of 2[OTf]$_2$, and its solubility in water reveals the H ⇋ D isotopic exchange undergone at the H8 site (Supporting Information).

The synthesis of **3** entails 2-fold C8-deprotonation of cation **2** and further coordination of both Ag^+ ions, which is unambiguously diagnosed by the absence of the H8 signals in its ^{1}H NMR spectrum (Figure 1). Further peak distribution is as follows: methyl groups from the theophylline scaffold appear as singlets at 4.27 (*N*9-CH_3), 3.84 (*N*3-CH_3) and 3.35 (*N*1-CH_3) ppm, whereas those of the acetate anions (*OAc*-CH_3) are observed at 1.90 ppm, confirming their coordination to the silver centers. Interestingly, *N*7-CH_2 and *O*-CH_2 resonate as broad pseudotriplets at 4.59 and 3.86 ppm. The

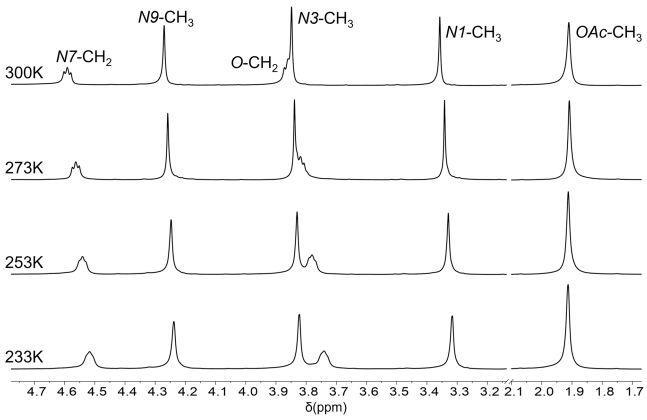

Figure 1. VT ^{1}H NMR spectra (CD_2Cl_2, 400 MHz) of **3**.

free rotation around the sigma single bonds of the seven-membered chain, (theophylline-*N*7)−CH_2−CH_2−O−CH_2−CH_2−(theophylline-*N*7), would render each CH_2 group chemically and magnetically equivalent, leading to pure triplets. However, the observed pseudotriplets, combined with the signal broadening, suggest hindered conformational rotation. This restriction increases the number of distinct energy states available for nuclear interactions, thus affecting the signal patterns.

This interpretation is corroborated by temperature-dependent ^{1}H NMR experiments, where cooling of the samples causes further signal broadening and noticeable chemical shift changes (Figure 1). Such behavior reflects a dynamic system influenced by temperature, likely due to conformational constraints imposed by the molecular structure and/or interactions.

The ^{13}C{^{1}H} NMR spectrum of **3** provides additional evidence of fluxional behavior. The C8 carbenic atom resonates as a singlet at 187.06 ppm. Besides, peaks corresponding to the acetate moiety are observed at 177.57 ppm (C13) and 22.56 ppm (C14). Typically, the presence of ^{107}Ag and ^{109}Ag isotopes would produce observable carbon−silver coupling doublets. However, their absence might indicate a nonrigid carbene-silver bond.[47,48] This fluxional nature is further suggested by the broadening of the methyl acetate peak (1.90 ppm) at room temperature.

To better understand the dynamic processes, ^{1}H DOSY NMR spectroscopy was employed, revealing a single species in solution with a hydrodynamic radius (r_H) of 4.63 Å (D = 1.10 × 10^{-9} m^2 s^{-1}). This finding supports the hypothesis that any dissociation or reformation of the Ag−C bond could occur rapidly on the NMR time scale at room temperature, maintaining the observed monomeric species in solution. Together, these results emphasize the interplay between hindered rotations, fluxionality, and rapid equilibria in defining the solution behavior of the Ag-nucleobase complex **3**.

Solid State Analysis. Compound **1** was crystallized by diffusion of diethyl ether into chloroform. After several days, single crystals of the hydrate **1**·0.25H_2O were obtained. The partial incorporation of water into the crystal lattice was attributed to the presence of moisture in the solvents. Its solid state structure (Figure 2) is consistent with that determined by ^{1}H NMR spectroscopy, where the −CH_2−CH_2−O−CH_2−CH_2− fragment is W-shaped and acts as a bridge between the two theophylline units, which are connected via their N7 sites. A notable feature of the geometry in compound **1** is that the C8−N7−C5 angles in both imidazole rings (105.86(15)°;

https://doi.org/10.1021/acs.inorgchem.4c05384
Inorg. Chem. 2025, 64, 5487−5494

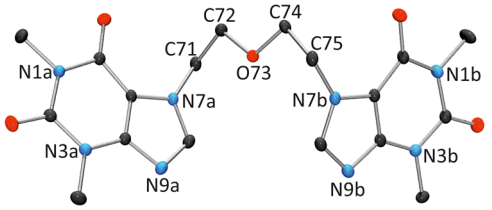

Figure 2. View of **1** with atom numbering scheme.

106.14(15)°) are larger than the corresponding C8−N9−C4 angles (103.22(15)°; 103.07(15)°), likely due to the coordination of the ether bridge at the latter positions.[46] In addition, both purine rings are mutually tilted by 34.87(3)°.

2-Fold methylation of compound **1** with methyl triflate afforded **2**$[OTf]_2$, whose structure was also determined by X-ray crystallography (Figure 3). Intermolecular bond distances

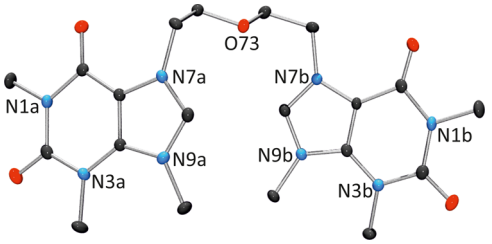

Figure 3. Front view of cation **2** in **2**$[OTf]_2$.

and angles are comparable to those of **1**, except for the endocyclic C−N−C angles within the imidazole rings, which in **2** exhibit identical values due to methylation at N9:[46] 107.77(19)° (C8a−N7a−C5a), 107.31(19)° (C8a−N9a−C4a), 107.45(19)° (C8b−N7b−C5b), and 107.55(19)° (C8b−N9b−C4b). Folding of cation **2** in **2**$[OTf]_2$ displays a slight deviation from that of **1**, with both nucleobases tilted by 11.12(10)° in a nearly antiparallel arrangement, with their C8 positions oriented toward each other.

Treatment of **2**$[OTf]_2$ with tetrabutylammonium bromide resulted in the formation of **2**$[Br]_2$, as described above. Interestingly, when **2**$[Br]_2$ was crystallized in methanolic media, crystals of the **2**$[Br]_2{\cdot}CH_3OH$ adduct were obtained. Although interatomic distances and angles of cation **2** in **2**$[Br]_2{\cdot}CH_3OH$ are almost identical to those in **2**$[OTf]_2$, its conformation differs. As depicted in Figure 4, cation **2** exhibits a U-conformation (C_s symmetry), accommodating a Br^- anion and a methanol molecule in its cavity, forming a host−guest

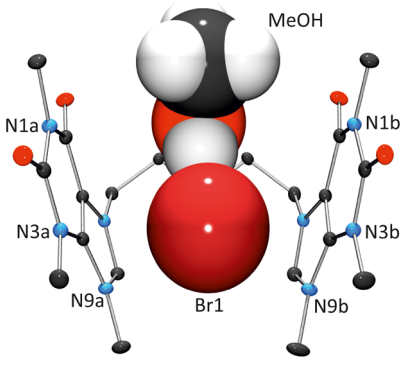

Figure 4. Detail of the host−guest system {Br,MeOH ⊂ **2**} in **2**$[Br]_2{\cdot}CH_3OH$. A Br^- anion has been omitted for clarity.

system, in which Br^- anion is connected by hydrogen bonding to methanol (MeOH···Br, 3.250(3) Å), and attached to the cationic host via electrostatics and anion−π interactions.

To use cation **2** as an NHC ligand precursor, the C8 position of the nucleobase was deprotonated by adding four equivalents of silver acetate to a suspension of **2**$[Br]_2$ in dichloromethane. As anticipated above, this treatment resulted in the coordination of a silver ion to each nucleobase via its C8 site, with the silver linear coordination sphere completed by an acetate ligand, forming $[Ag_2(OAc)_2(\mathbf{2}_{-2H})]$ (**3**). Compound **3** was initially isolated as a white, solvent-free powder. However, crystallization from a dimethyl sulfoxide (DMSO) solution yielded crystals that contained two solvent molecules in the asymmetric unit, identified as **3**·2DMSO.

Figure 5 provides a view of one enantiomer (see below) of **3** in **3**·2DMSO. The C_2 symmetry observed in NMR measure-

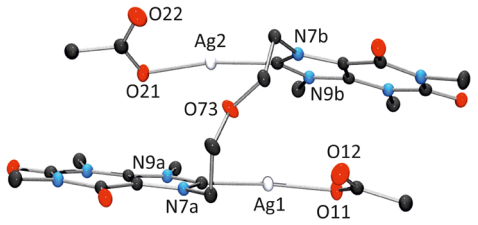

Figure 5. Side view of the (*P*)-**3** enantiomer in **3**·2DMSO. For *P*- and *M*-chirality see Figure 6.

ments is disrupted in the crystal structure. As a result, while the coordination environments of silver are analogous, they are not identical in the solid state. Bond distances involving Ag^+ ions are within the expected range: 2.083(3) Å (Ag1−C8a), 2.137(2) Å (Ag1−O11), 2.081(3) Å (Ag2−C8b), and 2.156(2) Å (Ag2−O21). In addition, separation between the two silver atoms is 3.9538(4) Å, which is probably too long to be considered a metallophilic interaction.[49] Coordination angles involving silver atoms deviate slightly from linearity: C8a−Ag1−O11, 170.78(10)°; (C8b−Ag2−O21), 170.42(10)°. Regarding its spatial conformation, complex **3** adopts an antiparallel orientation, similar to that of **2**$[OTf]_2$, with the C8 positions facing each other and a mutual tilt angle of 20.00(6)°. The acetate ligands are twisted relative to the nucleobases attached to the same silver atom, with torsion angles of 23.10(13)° (Ag1) and 34.85(16)° (Ag2). The uncoordinated oxygen atoms (O12, O22) point toward the Hoogsteen edges of the respective nucleobases.

More importantly, **3** crystallizes in two chiral isomers (Figure 6), *P* and *M*, both of which are present in the crystal packing of **3**·2DMSO. Both forms exhibit nearly identical (enantiomeric) arrangements, with the chirality of **3** in the solid state arising from its three-dimensional folding. To describe the two enantiomers of **3**, namely (*P*)-**3** and (*M*)-**3**, a scheme analogous to that employed for helicenes is utilized. As depicted in Figure 6 (left), a *P*-loop can be described starting at front-right acetate ligand, passing through its coordinated Ag and the adjoining nucleobase, then turning clockwise via the ether bridge to the other nucleobase, before reaching Ag′ and its attached back-left acetate ligand. A *M*-loop follows a counterclockwise rotation (Figure 6, right).

Remarkably, the crystal packing of the racemic solvate **3**·2DMSO exhibits a staggered arrangement, with π−π stacking interactions between symmetry-related nucleobases in an ···

https://doi.org/10.1021/acs.inorgchem.4c05384
Inorg. Chem. 2025, 64, 5487−5494

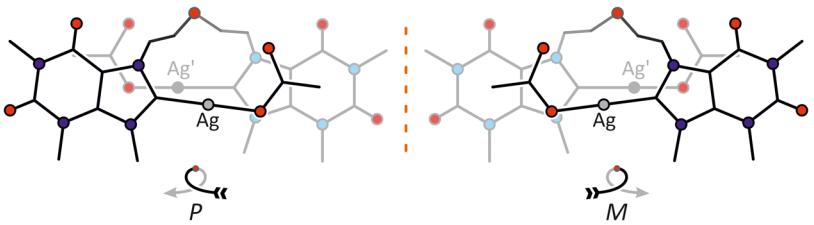

Figure 6. Conceptual depiction of the helical chirality exhibited by the (*P*)-**3** and (*M*)-**3** enantiomers in **3**·2DMSO.

M···*P*··· pattern (*M* and *P* refer to the different enantiomers of **3**), with stack distances of 3.4 Å (Figure 7).

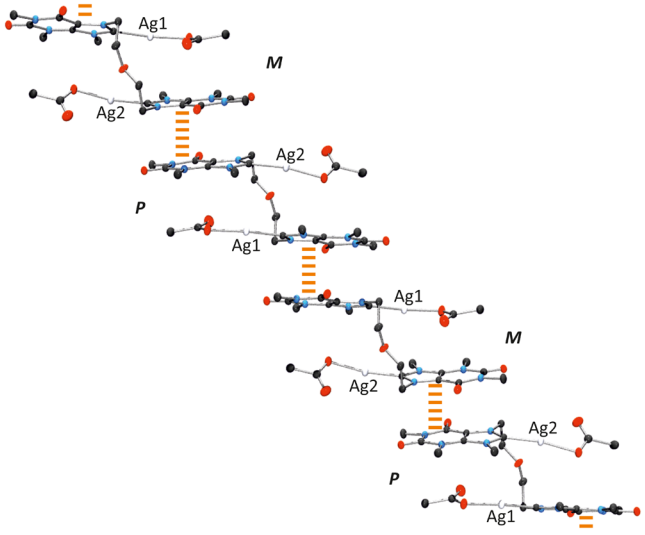

Figure 7. Staggered arrangement of **3** in **3**·2DMSO featuring $\pi-\pi$ stacking. For *P*- and *M*-chirality see Figure 6.

Further crystallization assays were carried out by diffusing hexane into solutions of **3** in either dichloromethane or chloroform. Here, the use of undried solvents (taken directly from the bottle) resulted in the formation of crystalline hydrates with the formula **3**·3H_2O. Thus, during the crystallization process, trace amounts of water are extracted from solvents, resulting in the formation of stable, durable crystals. Once the crystals have formed and the solvents are removed, they remain stable without any water loss for weeks when stored in air at room temperature.

Under the microscope, the resulting crystals appeared indistinguishable, differing only slightly in size and other expected characteristics. To determine the chirality of the crystals, they were manually selected and mounted onto a diffractometer for characterization. The first crystal selected for X-ray diffraction analysis was assigned to the trigonal $P3_121$ space group, and further identified as (*M*)-**3**·(*P*)-3H_2O, where *M* indicates the helicity of **3** (Figure 6) and *P* the helicity of the water chain (see below). Its absolute configuration was unambiguously established based on the Flack parameter: 0.029(8). In order to verify whether all the crystalline material exhibited the same chirality, several arbitrarily selected samples were analyzed. After multiple attempts, including X-ray measurements and refinements, we successfully identified a crystal that fitted within the $P3_221$ space group. The Flack parameter of 0.017(9) confirmed it as (*P*)-**3**·(*M*)-3H_2O, which is the enantiomer of (*M*)-**3**·(*P*)-3H_2O. Subsequent measurements of other picked crystals showed an equal distribution of the two enantiomers.

Hereinafter, only the crystal structure of (*M*)-**3**·(*P*)-3H_2O is described, as it is almost identical to that of (*P*)-**3**·(*M*)-3H_2O. In (*M*)-**3**·(*P*)-3H_2O, complex **3** exhibits a crystallographic C_2 axis that intersects the oxygen atom of the bridging ether, making the two halves of **3** symmetry-equivalent. Molecular arrangement of complex **3** in (*M*)-**3**·(*P*)-3H_2O is similar to that exhibited in **3**·2DMSO. However, while in the DMSO adduct the terminal oxygens of the acetate ligands are oriented toward the ether chain (Figure 6), in (*M*)-**3**·(*P*)-3H_2O and (*P*)-**3**·(*M*)-3H_2O, they are rotated by 180°, pointing instead toward sugar edges of the theophylline fragments (Supporting Information).

The unit cell of (*M*)-**3**·(*P*)-3H_2O contains complex **3** and two crystallographically different water molecules (O1w and O2w), both of which participate in hydrogen bonding, interacting with each other and/or with the acetate ligands. Hydrogen bonding distances are as follows: O1w···O1w′, 2.78(4) Å; O1w···O2w, 2.767(18) Å; O2w···O2w′, 2.878(16) Å; O1w···O12(acetate), 2.641(19) Å. In the crystal packing, the hydrogen bonding network between H_2O molecules organizes into helical, enantiopure one-dimensional water chains. Specifically, symmetry related O2w water molecules form a *P*-helix that twists around the *c* axis (Figure 8).

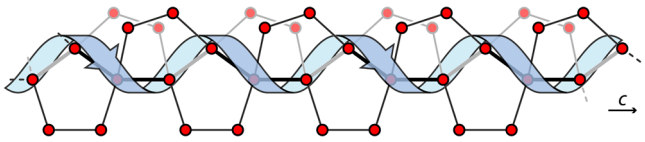

Figure 8. Schematic representation of the *P*-helical backbone within the water cluster of (*M*)-**3**·(*P*)-3H_2O. Red dot: oxygen atom.

The stability of this homochiral backbone is reinforced by envelope-like 5-membered water clusters, which surround the helix, and consist of three consecutive water molecules within the *P*-helix (O2w), along with two additional water molecules (O1w). The resulting fused pentagons form an intricate 1D array that preserves the *P*-helicity (Figure 8).

In addition, the cisoid arrangement of both acetate terminal oxygens toward the sugar edges allows complex **3** to bind the water cluster via 2-fold O1w···O12 (acetate) hydrogen bonds (Figure 9). These interactions are shorter than those involving water−water contacts (see above).

Remarkably, the helical arrangement of the water array induces an enantiospecific hydrogen bonding interaction with complex **3**, resulting in spontaneous chiral resolution. Such enantiomeric discrimination is not observed in the DMSO adduct. In particular, left-handed (*M*)-**3** units are attached to the right-handed (*P*) water chains to form (*M*)-**3**·(*P*)-3H_2O. In the case of the (*P*)-**3**·(*M*)-3H_2O, the contrary occurs, and

https://doi.org/10.1021/acs.inorgchem.4c05384
Inorg. Chem. 2025, 64, 5487−5494

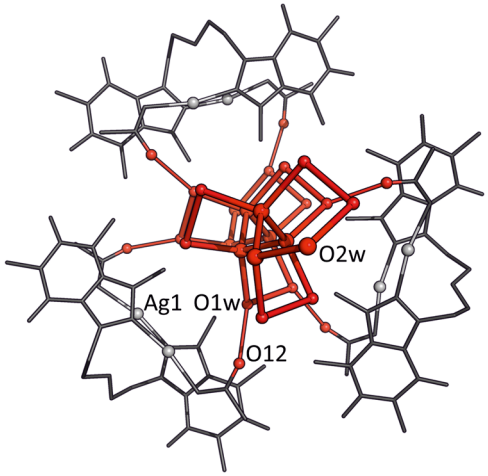

Figure 9. Detail of the helical arrangement of **3** in (*M*)-**3**·(*P*)-3H_2O around the respective chiral water chains.

right-handed complex (*P*)-**3** is recognized by the left-handed (*M*) water helix. Besides, positioning of silver complex **3** around the water chain results in a suprastructure that also maintains the helicity of the water cluster (Figure 10).

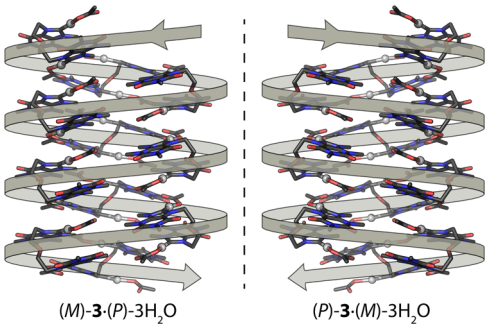

Figure 10. Two enantiomeric helical superstructures within the crystal packings of **3**·3H_2O.

To summarize, the transfer of chirality by a single achiral molecule is fundamentally limited. As demonstrated here, this situation changes when achiral molecules self-organize into supramolecular chiral assemblies. Such systems can generate chirality through interactions and molecular recognition, even in the absence of intrinsic chirality in the individual components.

CONCLUSIONS

The synthesis of the ether-nucleobase derivative **1** and the ditopic proligands **2**[OTf]$_2$ and **2**[Br]$_2$ facilitated the preparation of the silver-nucleobase complex **3**, which was crystallized in DMSO and in chlorinated solvents.

In crystals grown from DMSO, complex **3** adopts two enantiomeric isomers, namely *P* and *M*, which arise from rotation around the ether bridge. Within the crystal lattice, both enantiomers alternate in intermolecular $\pi-\pi$ interactions, stabilizing a racemic ladder-like structure. When crystallized from wet apolar solvents such as $CHCl_3$ or CH_2Cl_2, crystalline prisms of **3**·3H_2O assemble to achieve 1D helical water columns. Moreover, (*M*)-**3**·(*P*)-3H_2O crystallizes in the $P3_121$ space group, where **3** adopts *M*-chirality, while the water array exhibits *P*-helicity. In contrast, the enantiomeric crystal (*P*)-**3**·(*M*)-3H_2O is assigned to the $P3_221$ space group.

The crystal lattice of **3**·3H_2O is primarily stabilized by hydrogen bonding interactions, with other packing and intermolecular forces contributing to a lesser extent. This suggests that the arrangement of water molecules and their interactions with the silver complex **3** are fundamental to its structural integrity.

Therefore, chiral resolution of enantiomers during crystallization occurs spontaneously, without chiral auxiliaries. In this process, water drives the formation of enantiopure crystals, underscoring its pivotal role as a natural inducer of chirality. These findings offer fresh insights into stereochemical organization and highlight the unique ability of water to influence chiral outcomes in supramolecular assemblies.

EXPERIMENTAL SECTION

General Procedures. All the reagents used in this work were purchased from commercial sources and used as received. Glassware was dried at 140 °C before use. Unless otherwise stated, all reactions were carried out under aerobic conditions. CH_2Cl_2 was obtained oxygen- and waterfree from a Solvent Purification System (Innovative Technologies). Crystallization procedures were performed using undried solvents. ^1H and $^{13}C\{^1H\}$ NMR spectra were recorded on Bruker Avance 300 (300.13 and 75.48 MHz, respectively) and Bruker Avance 400 (400.16 and 100.61 MHz, respectively) spectrometers. Spectral assignments were achieved by combination of $^1H-^1H$ COSY, $^{13}C\{^1H\}$-APT and $^1H-^{13}C$ HSQC/HMBC. NMR chemical shifts (expressed in parts per million) are referenced to residual solvent peaks (^1H and ^{13}C). Methanol was used as internal standard in $^{13}C\{^1H\}$ and $^1H-^{13}C$ HSQC/HMBC spectra carried out in D_2O. Coupling constants, *J*, are given in hertz (Hz). High-resolution electrospray mass spectra (HRMS) were acquired using a MicroTOF-Q hybrid quadrupole time-of-flight spectrometer (Bruker Daltonics, Bremen, Germany). UV−visible spectra in solution were recorded on a JASCO V-670 UV−vis spectrophotometer.

X-ray diffraction data were collected on a Bruker D8 Venture diffractometer, using graphite-monochromated Mo Kα radiation (λ = 0.71073 Å). Diffracted intensities were integrated and corrected for absorption effects using the multiscan method.[50−52] Both procedures are included in the APEX4 package. All the structures were solved by direct methods with SHELXS[53] and refined by full-matrix least-squares on F^2 with SHELXL.[54]

Crystal Data for Compound ***1*****·0.25H_2O.** $C_{72}H_{90}N_{32}O_{21}$, M_r = 1739.75, colorless plate, monoclinic, *P*21/*c*, *a* = 7.2685(3) Å, *b* = 15.7196(6) Å, *c* = 17.4713(7) Å, β = 101.1997(13)°, *V* = 1958.22(14) Å^3, *Z* = 1, *T* = 100(2) K, D_{calcd} = 1.475 g cm^{-3}, μ = 0.112 mm^{-1}, absorption correction factors min. 0.090 max. 0.988, 69364 reflections, 4890 unique (R_{int} = 0.1032), 3432 observed, R_1 = 0.0491 [I > 2σ(I)], w$R_2(F^2)$ = 0.1322 (all data), GOF = 1.018. CCDC 2410723.

Crystal Data for Compound ***2*****[OTf]$_2$.** $C_{22}H_{28}F_6N_8O_{11}S_2$, M_r = 758.64, colorless prism, triclinic *P*−1, *a* = 9.4248(8) Å, *b* = 12.1373(11) Å, *c* = 13.4277(12) Å, α = 92.6242(12)°, β = 90.4004(12)°, γ = 103.6345(12)°, *V* = 1490.9(2) Å^3, *Z* = 2, *T* = 100(2) K, D_{calcd} = 1.690 g cm^{-3}, μ = 0.289 mm^{-1}, absorption correction factors min. 0.822 max. 0.918, 19195 reflections, 7261 unique (R_{int} = 0.0408), 5185 observed, R_1 = 0.0484 [I > 2σ(I)], w$R_2(F^2)$ = 0.1147 (all data), GOF = 1.041. CCDC 2410724.

Crystal Data for Compound ***2*****[Br]$_2$·CH_3OH.** $C_{21}H_{32}Br_2N_8O_6$, M_r = 652.36, colorless block, monoclinic *P*21/*c*, *a* = 8.4766(3) Å, *b* = 22.1517(6) Å, *c* = 14.5982(5) Å, β = 103.2819(13)°, *V* = 2667.80(15) Å^3, *Z* = 4, *T* = 100(2) K, D_{calcd} = 1.624 g cm^{-3}, μ = 3.091 mm^{-1}, absorption correction factors min. 0.739 max. 0.790, 109976 reflections, 6638 unique (R_{int} = 0.0456), 6088 observed, R_1 = 0.0333 [I > 2σ(I)], w$R_2(F^2)$ = 0.0938 (all data), GOF = 1.069. CCDC 2410725.

https://doi.org/10.1021/acs.inorgchem.4c05384
Inorg. Chem. 2025, 64, 5487−5494

Crystal Data for Compound **3**·*2DMSO.* $C_{28}H_{44}Ag_2N_8O_{11}S_2$, M_r = 948.57, colorless block, monoclinic *P*21/*c*, *a* = 20.1200(11) Å, *b* = 8.5680(5) Å, *c* = 22.0957(12) Å, *β* = 106.777(2)°, *V* = 3646.9(4) Å^3, *Z* = 4, *T* = 100(2) K, D_{calcd} = 1.728 g cm^{-3}, *μ* = 1.256 mm^{-1}, absorption correction factors min. 0.727 max. 0.828, 107317 reflections, 9107 unique (R_{int} = 0.0511), 7984 observed, R_1 = 0.0354 [I > 2*σ*(I)], w$R_2(F^2)$ = 0.0899 (all data), GOF = 1.158. CCDC 2410726.

*Crystal Data for Compound (M)-***3**·*(P)-3H$_2$O.* $C_{24}H_{38}Ag_2N_8O_{12}$, M_r = 846.36, colorless prism, trigonal *P*3121, *a* = 19.5911(6) Å, *c* = 7.0016(3) Å, *V* = 2327.26(17)Å^3, *Z* = 3, *T* = 100(2) K, D_{calcd} = 1.812 g cm^{-3}, *μ* = 1.336 mm^{-1}, absorption correction factors min. 0.842 max. 0.899, 75560 reflections, 3880 unique (R_{int} = 0.0545), 3763 observed, R_1 = 0.0938 [I > 2*σ*(I)], w$R_2(F^2)$ = 0.1966 (all data), GOF = 1.092. CCDC 2410727.

*Crystal Data for Compound (M)-***3**·*(P)-3H$_2$O.* $C_{24}H_{38}Ag_2N_8O_{12}$, M_r = 846.36, colorless prism, trigonal *P*3221, *a* = 19.5955(4) Å, *c* = 7.0045(3) Å, *V* = 2329.27(14) Å^3, *Z* = 3, *T* = 100(2) K, D_{calcd} = 1.810 g cm^{-3}, *μ* = 1.335 mm^{-1}, absorption correction factors min. 0.805 max. 0.923, 90779 reflections, 3878 unique (R_{int} = 0.0553), 3729 observed, R_1 = 0.0902 [I > 2*σ*(I)], w$R_2(F^2)$ = 0.2029 (all data), GOF = 1.097. CCDC 2410728.

Synthesis of Bis(theophylline-*N*7-ethyl)ether, 1. Theophylline (3.30 g, 18.3 mmol) and NaOH (1.06 g, 26.5 mmol) were suspended in 20 mL of DMF and the mixture was heated to 50 °C. Then, bis(2-chloroethyl) ether (1.3 mL, 11.1 mmol) was added and the temperature was raised to 80 °C. After 40 h the mixture was cooled down to room temperature and 20 mL of water were added. The white suspension was filtered, washed with water (2 × 10 mL) and methanol (2 × 5 mL) and dried under vacuum to yield **1** as a white solid (3.00 g, 76%). ^{1}H NMR (400 MHz, $CDCl_3$, 298 K): *δ* 7.40 (s, 2H, H8), 4.37 (t, $^3J_{H-H}$ = 4.5 Hz, 4H, *N*7-CH_2), 3.71 (t, $^3J_{H-H}$ = 4.5 Hz, 4H, *O*-CH_2), 3.55 (s, 6H, *N*3-CH_3), 3.34 (s, 6H, *N*1-CH_3). ^{13}C{^{1}H} NMR (100 MHz, $CDCl_3$, 298 K): *δ* 155.30 (C6), 151.63 (C2), 149.08 (C4), 141.93 (C8), 106.56 (C5), 69.38 (*O*-C), 46.89 (*N*7-C), 29.88 (*N*3-C), 28.02 (*N*1-C). HRMS ($CHCl_3$/CH_3CN) [M + Na]$^+$ calcd. for $C_{18}H_{22}N_8O_5Na$: 453.1605; found: 453.1603.

Synthesis of Bis(theophylline-*N*9-methyl-*N*7-ethyl)ether Triflate, 2[OTf]$_2$. Under argon atmosphere, methyl trifluoromethanesulfonate (0.75 mL, 6.65 mmol) was added to a suspension of **1** (1.00 g, 2.34 mmol) in 20 mL of dry dichloromethane and the mixture was stirred at room temperature. The suspension gradually disappeared upon 1 h of stirring, giving rise to a colorless solution. Shortly after, a white precipitate appeared, and the mixture was stirred at room temperature for 3 days. Filtration and washings with dichloromethane (2 × 10 mL) and diethyl ether (3 × 10 mL) afforded **2**[OTf]$_2$ as a white solid (1.56 g, 2.06 mmol, 88%). ^{1}H NMR (400 MHz, CD_3CN, 298 K): *δ* 8.79 (s, 2H, H8), 4.67 (t, $^3J_{H-H}$ = 4.8 Hz, 4H, *N*7-CH_2), 4.14 (s, 6H, *N*9-CH_3), 3.81 (t, $^3J_{H-H}$ = 4.8 Hz, 4H, *O*-CH_2), 3.74 (s, 6H, *N*3-CH_3), 3.31 (s, 6H, *N*1-CH_3). ^{13}C{^{1}H} NMR (100 MHz, CD_3CN, 298 K): *δ* 154.75 (C6), 151.45 (C2), 140.83 (C4), 140.11 (C8), 108.80 (C5), 68.63 (*O*-C), 49.83 (*N*7-C), 38.09 (*N*9-C), 32.22 (*N*3-C), 29.14 (*N*1-C). ^{19}F NMR (282 MHz, CD_3CN, 298 K): *δ* −79.40 (s, OTf). HRMS (CH_3CN) [M − 2OTf]$^{2+}$ calcd. for $C_{20}H_{28}N_8O_5$: 230.1086; found: 230.1093/[M − OTf]$^+$ calcd. for $C_{21}H_{28}N_8O_8SF_3$: 609.1697; found: 609.1727.

Synthesis of Bis(theophylline-*N*9-methyl-*N*7-ethyl)ether Bromide, 2[Br]$_2$. **2**[OTf]$_2$ (298 mg, 0.39 mmol) was suspended in 15 mL of THF and tetrabutylammonium bromide (326 mg, 1.01 mmol) was added. After stirring at room temperature for 15 h, the white precipitate was filtered off, washed with further THF and acetone (2 × 5 mL) and dried under vacuum to yield **2**[Br]$_2$ as a white solid (240 mg, 0.38 mmol, 98%). ^{1}H NMR (300 MHz, D_2O, 298 K): *δ* 4.75 (t, $^3J_{H-H}$ = 4.9 Hz, 4H, *N*7-CH_2), 4.24 (s, 6H, *N*9-CH_3), 3.96 (t, $^3J_{H-H}$ = 4.9 Hz, 4H, *O*-CH_2), 3.83 (s, 6H, *N*3-CH_3), 3.37 (s, 6H, *N*1-CH_3). ^{13}C{^{1}H} NMR (100 MHz, D_2O, 298 K): *δ* 155.12 (C6), 152.09 (C2), 140.46 (C4), 140.12 (t, $^1J_{C-D}$ = 30.0 Hz, C8), 108.84 (C5), 68.64 (*O*-C), 49.25 (*N*7-C), 37.93 (*N*9-C), 32.38 (*N*3-C), 29.31 (*N*1-C). HRMS (CH_3OH) [M − 2Br]$^{2+}$ calcd. for $C_{20}H_{28}N_8O_5$: 230.1086; found: 230.1093/[M − Br]$^+$ calcd. for $C_{20}H_{28}N_8O_5Br$: 541.1343; found: 541.1349.

Synthesis of 3. **2**[Br]$_2$ (111 mg, 0.18 mmol) was suspended in 12 mL of dichloromethane and silver acetate (129 mg, 0.77 mmol) was added. The white precipitate gradually transformed into a yellowish suspension in the span of 15 min. After stirring overnight, the yellow solid was removed upon filtration through Celite and the colorless solution was concentrated to about 1 mL under reduced pressure. Addition of 10 mL of hexane afforded a white solid which was filtered, washed with further hexane (2 × 5 mL) and dried under vacuum (110 mg, 0.14 mmol, 77%). ^{1}H NMR (400 MHz, CD_2Cl_2, 298 K): 4.59 (pt, $^3J_{H-H}$ = 4.2 Hz, 4H, *N*7-CH_2), 4.27 (s, 6H, *N*9-CH_3), 3.86 (br-pt, 4H, *O*-CH_2), 3.84 (s, 6H, *N*3-CH_3), 3.35 (s, 6H, *N*1-CH_3), 1.90 (s, 6H, *OAc*-CH_3). ^{13}C{^{1}H} NMR (100 MHz, CD_2Cl_2, 298 K): 187.06 (C8), 177.57 (C13), 154.03 (C6), 151.32 (C2), 141.41 (C4), 109.46 (C5), 69.27 (*O*-C), 52.19 (*N*7-C), 40.47 (*N*9-C), 32.32 (*N*3-C), 28.99 (*N*1-C), 22.56 (C14). HRMS ($CDCl_3$/CH_3OH) [M − Ag − 2 OAc]$^+$ calcd. for $C_{20}H_{26}N_8O_5Ag$: 565.1072; found: 565.1049.

■ ASSOCIATED CONTENT

Supporting Information

The Supporting Information is available free of charge at https://pubs.acs.org/doi/10.1021/acs.inorgchem.4c05384.

1D and 2D NMR spectra for all compounds (PDF)

Accession Codes

Deposition Numbers 2410723−2410728 contain the supplementary crystallographic data for this paper. These data can be obtained free of charge via the joint Cambridge Crystallographic Data Centre (CCDC) and Fachinformationszentrum Karlsruhe Access Structures service.

■ AUTHOR INFORMATION

Corresponding Author

Pablo J. Sanz Miguel − *Departamento de Química Inorgánica, Instituto de Síntesis Química y Catálisis Homogénea (ISQCH), Universidad de Zaragoza-CSIC, Zaragoza 50009, Spain;* orcid.org/0000-0002-8220-6031; Email: pablo.sanz@unizar.es

Authors

Alvaro Polo − *Departamento de Química Inorgánica, Instituto de Síntesis Química y Catálisis Homogénea (ISQCH), Universidad de Zaragoza-CSIC, Zaragoza 50009, Spain*

Ricardo Rodríguez − *Departamento de Química Inorgánica, Instituto de Síntesis Química y Catálisis Homogénea (ISQCH), Universidad de Zaragoza-CSIC, Zaragoza 50009, Spain;* orcid.org/0000-0002-8845-0174

Ramón Macías − *Departamento de Química Inorgánica, Instituto de Síntesis Química y Catálisis Homogénea (ISQCH), Universidad de Zaragoza-CSIC, Zaragoza 50009, Spain;* orcid.org/0000-0003-2299-9428

Daniel Cobo Paz − *Departamento de Química Inorgánica, Instituto de Síntesis Química y Catálisis Homogénea (ISQCH), Universidad de Zaragoza-CSIC, Zaragoza 50009, Spain*

Complete contact information is available at: https://pubs.acs.org/10.1021/acs.inorgchem.4c05384

Notes

The authors declare no competing financial interest.

■ ACKNOWLEDGMENTS

Financial support from the University of Zaragoza, the Aragón Government (A.P. predoctoral fellow, E42_23R, E05_23R),

and the MCIU/AEI/FEDER (PID2021-122406NB-I00 and PID2022-137208NB-I00) is kindly acknowledged.

REFERENCES

(1) Latimer, W. M.; Rodebush, W. H. Polarity and ionization from the standpoint of the Lewis Theory of Valence. *J. Am. Chem. Soc.* **1920**, *42* (7), 1419−1433.
(2) Ludwig, R. Water: From Clusters to the Bulk. *Angew. Chem., Int. Ed.* **2001**, *40*, 1808−1827.
(3) Wang, B.; Jiang, W.; Dai, X.; Gao, Y.; Wang, Z.; Zhang, R.-Q. Molecular orbital analysis of the hydrogen bonded water dimer. *Sci. Rep.* **2016**, *6* (1), 22099.
(4) Liu, K.; Cruzan, J. D.; Saykally, R. J. Water clusters. *Science* **1996**, *271*, 929−933.
(5) Keutsch, F. N.; Saykally, R. J. Water clusters: Untangling the mysteries of the liquid, one molecule at a time. *Proc. Natl. Acad. Sci. U.S.A.* **2001**, *98*, 10533−10540.
(6) Eisenberg, D.; Kauzmann, W. *The Structure and Properties of Water*; Oxford University Press, 2005.
(7) Infantes, L.; Motherwell, S. Water clusters in organic molecular crystals. *CrystEngcomm* **2002**, *4*, 454−461.
(8) Wei, D. G.; Wilson, W. D.; Neidle, S. Small-molecule Binding to the DNA Minor Groove Is Mediated by a Conserved Water Cluster. *J. Am. Chem. Soc.* **2013**, *135*, 1369−1377.
(9) Pullanchery, S.; Roke, S. Handy water: Chiral superstructures around peptide β-sheets. *Proc. Natl. Acad. Sci. U.S.A.* **2021**, *118* (2), No. e2024376118.
(10) Steber, A. L.; Temelso, D.; Kisiel, Z.; Schnell, M.; Pérez, C. Rotational dive into the water clusters on a simple sugar substrate. *Proc. Natl. Acad. Sci. U.S.A.* **2023**, *120*, No. e2214970120.
(11) Jayaram, B.; Jain, T. The role of water in protein-DNA recognition. *Annu. Rev. Biophys. Biomol. Struct.* **2004**, *33*, 343−361.
(12) Ball, P. Water as an Active Constituent in Cell Biology. *Chem. Rev.* **2008**, *108*, 74−108.
(13) Zhong, D.; Pal, S. K.; Zewail, A. H. Biological water: A critique. *Chem. Phys. Lett.* **2011**, *503*, 1−11.
(14) Duboué-Dijon, E.; Fogarty, A. C.; Hynes, J. T.; Laage, D. Dynamical Disorder in the DNA Hydration Shell. *J. Am. Chem. Soc.* **2016**, *138*, 7610−7620.
(15) Kocsis, I.; Sorci, M.; Vanselous, H.; Murail, S.; Sanders, S. E.; Licsandru, E.; Legrand, Y.-M.; van der Lee, A.; Baaden, M.; Petersen, P. B.; et al. Oriented chiral water wires in artificial transmembrane channels. *Sci. Adv.* **2018**, *4*, No. eaao5603.
(16) Su, D.-D.; Barboiu, M. Hydrogen-bonded water-wires/clusters − Toward natural selectivity of artificial water channels. *Coord. Chem. Rev.* **2024**, *515*, 215973.
(17) Perets, E. A.; Yan, E. C. Y. The H_2O Helix: The Chiral Water Superstructure Surrounding DNA. *ACS Cent. Sci.* **2017**, *3*, 683−685.
(18) McDermott, M. L.; Vanselous, H.; Corcelli, S. A.; Petersen, P. B. DNA's Chiral Spine of Hydration. *ACS Cent. Sci.* **2017**, *3*, 708−714.
(19) Kumar, N.; Khullar, S.; Mandal, S. K. Encapsulation of a Water Octamer Chain in a Chiral 2D Sheetlike Supramolecular Coordination Network Composed of Dinickel-Dicarboxylate Subunits. *ACS Omega* **2018**, *3*, 11062−11070.
(20) Wu, B.; Wang, S.; Wang, R.; Xu, J.; Yuan, D.; Hou, H. Chiral Metallocycles Templated Novel Chiral Water Frameworks. *Cryst. Growth Des.* **2013**, *13*, 518−525.
(21) Han, L.-L.; Zhang, X.-Y.; Chen, J.-S.; Li, Z.-H.; Sun, D.-F.; Wang, X.-P.; Sun, D. Silver(I)/Bipyrazole/Dicarboxylate Interpenetrated Coordination Networks: Spontaneous Chiral Resolution, Modulation of Topologies, Water Clusters, and Photoluminescences. *Cryst. Growth Des.* **2014**, *14*, 2230−2239.
(22) Ganguly, S.; Mondal, R. Coordination Driven Self-Assembly in Co(II) Coordination Polymers Displaying Unprecedented Topology, Water Cluster, Chirality, and Spin-Canted Magnetic Behavior. *Cryst. Growth Des.* **2015**, *15*, 2211−2222.
(23) Otake, K.-I.; Otsubo, K.; Komatsu, T.; Dekura, S.; Taylor, J. M.; Ikeda, R.; Sugimoto, K.; Fujiwara, A.; Chou, C.-P.; Sakti, A. W.; et al. Confined water-mediated high proton conduction in hydrophobic channel of a synthetic nanotube. *Nat. Commun.* **2020**, *11* (1), 843.
(24) Tang, X.; Chu, D.; Jiang, H.; Gong, W.; Jiang, C.; Cui, Y.; Liu, Y. Supramolecular self-assembly of chiral helical tubular polymers with amplified circularly polarized luminescence. *Mater. Chem. Front.* **2020**, *4*, 2772−2781.
(25) Tan, K. T.; Tao, S.; Huang, N.; Jiang, D. Water cluster in hydrophobic crystalline porous covalent organic frameworks. *Nat. Commun.* **2021**, *12* (1), 6747.
(26) Yuan, G.; Zhu, C.; Liu, Y.; Fang, Y.; Cui, Y. Water clusters induced assembly of chiral organic microstructures showing reversible phase transformations and luminescence switching. *Chem. Commun.* **2010**, *46*, 2307−2309.
(27) Brackemeyer, D.; Hervé, A.; To Brinke, C. S.; Jahnke, M. C.; Hahn, F. E. A Versatile Methodology for the Regioselective C8-Metalation of Purine Bases. *J. Am. Chem. Soc.* **2014**, *136*, 7841−7844.
(28) Leitao, M. I. P. S.; Gonzalez, C.; Francescato, G.; Filipiak, Z.; Petronilho, A. On the reactivity of mRNA Cap0: C−H oxidative addition of 7-methylguanosine to Pt^0 and base pairing studies. *Chem. Commun.* **2020**, *56*, 13365−13368.
(29) Odena, C.; Santiago, T. G.; Linares, M. L.; Castellanos-Blanco, N.; McGuire, R. T.; Chaves-Arquero, B.; Alonso, J. M.; Diéguez-Vázquez, A.; Tan, E.; Alcázar, J.; Buijnsters, P.; Cañellas, S.; Martin, R. Late-Stage $C(sp^2)$-$C(sp^3)$ Diversification via Nickel Oxidative Addition Complexes. *J. Am. Chem. Soc.* **2024**, *146*, 21264−21270.
(30) Kascatan-Nebioglu, A.; Melaiye, A.; Hindi, K.; Durmus, S.; Panzner, M. J.; Hogue, L. A.; Mallett, R. J.; Hovis, C. E.; Coughenour, M.; Crosby, S. D.; Milsted, A.; Ely, D. L.; Tessier, C. A.; Cannon, C. L.; Youngs, W. J. Synthesis from Caffeine of a Mixed N-Heterocyclic Carbene-Silver Acetate Complex Active against Resistant Respiratory Pathogens. *J. Med. Chem.* **2006**, *49*, 6811−6818.
(31) Bertrand, B.; Stefan, L.; Pirrotta, M.; Monchaud, D.; Bodio, E.; Richard, P.; Le Gendre, P.; Warmerdam, E.; de Jager, M. H.; Groothuis, G. M. M.; Picquet, M.; Casini, A. Caffeine-Based Gold(I) N-Heterocyclic Carbenes as Possible Anticancer Agents: Synthesis and Biological Properties. *Inorg. Chem.* **2014**, *53*, 2296−2303.
(32) Meier-Menches, S. M.; Neuditschko, B.; Zappe, K.; Schaier, M.; Gerner, M. C.; Schmetterer, K. G.; Del Favero, G.; Bonsignore, R.; Cichna-Markl, M.; Koellensperger, G.; et al. An Organometallic Gold(I) Bis-N-Heterocyclic Carbene Complex with Multimodal Activity in Ovarian Cancer Cells. *Chem. - Eur. J.* **2020**, *26*, 15528−15537.
(33) Francescato, G.; Leitão, M. I. P. S.; Orsini, G.; Petronilho, A. Synthesis and Medicinal Applications of N-Heterocyclic Carbene Complexes Based on Caffeine and Other Xanthines. *ChemMedchem* **2024**, *19*, No. e202400118.
(34) Zhang, J.-J.; Muenzner, J. K.; el Maaty, M. A. A.; Karge, B.; Schobert, R.; Wölfl, S.; Ott, I. A multi-target caffeine derived rhodium(I) N-heterocyclic carbene complex: Evaluation of the mechanism of action. *Dalton Trans.* **2016**, *45*, 13161−13168.
(35) Kaußler, C.; Wragg, D.; Schmidt, C.; Moreno-Alcántar, G.; Jandl, C.; Stephan, J.; Fischer, R. A.; Leoni, S.; Casini, A.; Bonsignore, R. Dynamical Docking" of Cyclic Dinuclear Au(I) Bis-N-heterocyclic Complexes Facilitates Their Binding to G-Quadruplexes. *Inorg. Chem.* **2022**, *61*, 20405−20423.
(36) Mazars, F.; Delaude, L. Greening" Ruthenium-Arene Catalyst Precursors with N-Heterocyclic Carbene Ligands Derived from Caffeine and Theophylline. *Organometallics* **2023**, *42*, 1589−1597.
(37) Zhang, J.; Rahman, M. M.; Zhao, Q.; Feliciano, J.; Bisz, E.; Dziuk, B.; Lalancette, R.; Szostak, R.; Szostak, M. N-Heterocyclic Carbene Complexes of Nickel(II) from Caffeine and Theophylline: Sustainable Alternative to Imidazol-2-ylidenes. *Organometallics* **2022**, *41*, 1806−1815.
(38) Szadkowska, A.; Staszko, S.; Zaorska, E.; Pawłowski, R. A theophylline based copper N-heterocyclic carbene complex: Synthesis and activity studies in green media. *RSC Adv.* **2016**, *6*, 44248−44253.
(39) Bysewski, O.; Klosterhalfen, N.; Jordan, R.; Kletsch, L.; Winter, A.; Klein, A.; Dietzek-Ivanšić, B.; Schubert, U. S. Luminescent Platinum(II) Complexes with a Tridentate Caffeine-Based NHC-

https://doi.org/10.1021/acs.inorgchem.4c05384
Inorg. Chem. 2025, 64, 5487−5494

Pincer Ligand: Synthesis, Electrochemistry and Photophysics. *Eur. J. Inorg. Chem.* **2024**, *27* (5), No. e202300620.
(40) Chaudhary, A.; Mathur, D.; Gaba, R.; Pasricha, R.; Sharma, K. Greening up organic reactions with caffeine: Applications, recent developments, and future directions. *RSC Adv.* **2024**, *14*, 8932−8962.
(41) Vellé, A.; Cebollada, A.; Iglesias, M.; Sanz Miguel, P. J. Argentophilicity as Essential Driving Force for a Dynamic Cation-Cation Host-Guest System: $[Ag(acetonitrile)_2]^+ \subset [Ag_2(bis\text{-}NHC)_2]^{2+}$ (NHC = *N*-heterocyclic carbene). *Inorg. Chem.* **2014**, *53*, 10654−10659.
(42) Cebollada, A.; Vellé, A.; Iglesias, M.; Fullmer, L. B.; Goberna-Ferrón, S.; Nyman, M.; Sanz Miguel, P. J. Direct X-Ray Scattering Evidence for Metal−Metal Interactions in Solution at the Molecular Level. *Angew. Chem., Int. Ed.* **2015**, *54*, 12762−12766.
(43) Vellé, A.; Rodríguez-Santiago, L.; Sodupe, M.; Sanz Miguel, P. J. Enhanced Metallophilicity in Metal-Carbene Systems: Stronger Character of Aurophilic Interactions in Solution. *Chem. - Eur. J.* **2020**, *26*, 997−1002.
(44) Quintana, M.; Rodríguez-Rius, A.; Vellé, A.; Vives, S.; Sanz Miguel, P. J.; Triola, G. Dinuclear silver and gold bisNHC complexes as drug candidates for cancer therapy. *Bioorg. Med. Chem.* **2022**, *67*, 116814.
(45) Polo, A.; Gutiérrez Merino, L.; Rodríguez, R.; Sanz Miguel, P. J. Chirality at Metal in a Linear $[Ag(NHC)_2]^+$ Complex: Stereogenic C−Ag−C Axis, Atropisomerism and Role of π-π Interactions. *Chem. - Eur. J.* **2024**, *30*, No. e202403239.
(46) Vellé, A.; Cebollada, A.; Macías, R.; Iglesias, M.; Gil-Moles, M.; Sanz Miguel, P. J. From Imidazole toward Imidazolium Salts and N-Heterocyclic Carbene Ligands: Electronic and Geometrical Redistribution. *ACS Omega* **2017**, *2*, 1392−1399.
(47) Kascatan-Nebioglu, A.; Panzner, M. J.; Garrison, J. C.; Tessier, C. A.; Youngs, W. J. Synthesis and Structural Characterization of *N*-Heterocyclic Carbene Complexes of Silver(I) and Rhodium(I) from Caffeine. *Organometallics* **2004**, *23*, 1928−1931.
(48) Wang, H. M. J.; Lin, I. J. B. Facile Synthesis of Silver(I)-Carbene Complexes. Useful Carbene Transfer Agents. *Organometallics* **1998**, *17*, 972−975.
(49) Schmidbaur, H.; Schier, A. Argentophilic Interactions. *Angew. Chem., Int. Ed.* **2015**, *54*, 746−784.
(50) Bruker. *Area-Detector Integration Software, version 6.01*; Bruker, Madison, 2001.
(51) Bruker. *Area Detector Absorption Program*, Bruker, Madison, WI, 1996.
(52) Krause, L.; Herbst-Irmer, R.; Sheldrick, G. M.; Stalke, D. Comparison of silver and molybdenum microfocus X-ray sources for single-crystal structure determination. *J. Appl. Crystallogr.* **2015**, *48*, 3−10.
(53) Sheldrick, G. M. A short history of SHELX. *Acta Crystallogr., Sect. A:Found. Crystallogr.* **2008**, *A64*, 112−122.
(54) Sheldrick, G. M. Crystal structure refinement with SHELXL. *Acta Crystallogr., Sect. C: Struct. Chem.* **2015**, *71*, 3−8.

https://doi.org/10.1021/acs.inorgchem.4c05384
Inorg. Chem. 2025, 64, 5487−5494